• Basic Research •

Neuroprotective effects of acteoside in a glaucoma mouse model by targeting Serta domain-containing protein 4

Hui-Jie Hao, Ya-Hong Li, Bo Yu, Xun Liu, Yan Zhang, Xiao-Li Xing

Tianjin Key Laboratory of Retinal Functions and Diseases, Tianjin Branch of National Clinical Research Center for Ocular Disease, Eye Institute and School of Optometry, Tianjin Medical University Eye Hospital, Tianjin 300384, China

Correspondence to: Yan Zhang and Xiao-Li Xing. Tianjin Key Laboratory of Retinal Functions and Diseases, Tianjin Branch of National Clinical Research Center for Ocular Disease, Eye Institute and School of Optometry, Tianjin Medical University Eye Hospital, Tianjin 300384, China. yanzhang04@tmu.edu.cn; xxlteh@126.com

Received: 2023-07-26 Accepted: 2024-01-04

Abstract

● **AIM:** To explore the therapeutic effect and main molecular mechanisms of acteoside in a glaucoma model in DBA/2J mice.

● **METHODS:** Proteomics was used to compare the differentially expressed proteins of C57 and DBA/2J mice. After acteoside administration in DBA/2J mice, anterior segment observation, intraocular pressure (IOP) monitoring, electrophysiology examination, and hematoxylin and eosin staining were used to analyze any potential effects. Immunohistochemistry (IHC) assays were used to verify the proteomics results. Furthermore, retinal ganglion cell 5 (RGC5) cell proliferation was assessed with cell counting kit-8 (CCK-8) assays. Serta domain-containing protein 4 (Sertad4) mRNA and protein expression levels were measured by qRT-PCR and Western blot analysis, respectively.

● **RESULTS:** Proteomics analysis suggested that Sertad4 was the most significantly differentially expressed protein. Compared with the saline group, the acteoside treatment group showed decreased IOP, improved N1-P1 wave amplitudes, thicker retina, and larger numbers of cells in the ganglion cell layer (GCL). The IHC results showed that Sertad4 expression levels in DBA/2J mice treated with acteoside were significantly lower than in the saline group. Acteoside treatment could improve RGC5 cell survival and reduce the Sertad4 mRNA and protein expression levels after glutamate injury.

● **CONCLUSION:** Sertad4 is differentially expressed in DBA/2J mice. Acteoside can protect RGCs from damage, possibly through the downregulation of Sertad4, and has a potential use in glaucoma treatment.

● **KEYWORDS:** glaucoma; acteoside; Serta domain-containing protein 4; proteomics; mice

DOI:10.18240/ijo.2024.04.04

Citation: Hao HJ, Li YH, Yu B, Liu X, Zhang Y, Xing XL. Neuroprotective effects of acteoside in a glaucoma mouse model by targeting Serta domain-containing protein 4. *Int J Ophthalmol* 2024;17(4):625-637

INTRODUCTION

Glaucoma is an irreversible blinding eye disease that has traditionally been regarded as a stress-induced neurodegenerative disease[1]. Glaucoma is mainly characterized by retinal ganglion cell (RGC) loss, optic nerve damage, and visual field defects. A gradual elevation of intraocular pressure (IOP) can lead to vision loss[2], and high IOP also results in the loss of large numbers of RGCs[3], which is an irreversible process. Therefore, glaucoma treatment development has focused on reducing IOP. However, controlling IOP alone does not entirely prevent RGC loss[4]. Persistent deterioration of optic nerve function may occur after treatment, so protection of RGC damage is also key to glaucoma treatment.

The conventional treatment methods for glaucoma include drugs, laser therapy, and surgery[5]. Acteoside is a naturally occurring water-soluble compound found in natural products and plant extracts. It is abundant in many dicotyledonous plants, such as oleaceae, verbena, and lamiaceae[6]. Acteoside is easily hydrolyzed in the digestive tract and can decompose into various products that are absorbed into the blood before being degraded[7]. As a bioactive natural ingredient, acteoside possesses beneficial pharmacological activities for human health, including anti-apoptosis, anti-inflammatory[8], antioxidant[9], anti-cancer[10], wound healing, and neuroprotective properties[11]. Evidence has suggested that acteoside has anti-inflammatory effects and can alleviate

neurological and respiratory symptoms after COVID-19 infection[12]. Acteoside may improve unilateral ureteral obstruction (UUO)-induced renal inflammation and fibrosis in rats by triggering the HMGN1/TLR4/TREM-1 pathway[13] and can be used to treat chronic glomerulonephritis[14]. In addition, acteoside can attenuate lung injury[15]. Supplementing acteoside can protect the eye from natural oxidation[16]. Different liposome preparations containing acteoside can be used to treat alkali-induced corneal epithelial burns[17]. *In vitro* experiments with glioblastoma cell lines showed that liposome-encapsulated acteoside has potential as an anti-cancer drug[18]. Acteoside in *Cistanche deserticola* plays a protective role in bone by activating the PI3K/AKT/mTOR signaling pathway to alleviate dexamethasone-induced osteoporosis[19]. Acteoside plays an active role in a Parkinson's disease (PD) model and can alleviate salsolinol-induced pyroptosis-dependent neurotoxicity[20]. Acteoside may act as a neuroprotective drug against ocular disease, but there are currently few studies that have examined this.

Glaucoma is also considered to be a neurodegenerative disease, and growing evidence suggests that neuroprotective strategies may be effective treatment approaches for this disease[21-22]. The neuroprotective function of acteoside can possibly be applied as a potential drug to protect glaucoma-associated RGC damage. Proteomics is an important method for exploring differentially expressed proteins associated with various diseases and has been widely used in the eye[23-25]. Proteomics can be applied to clarify the molecular mechanisms of glaucoma, which remain uncertain[26]. The main molecular mechanism of the DBA/2J spontaneous glaucoma mouse model, in which acteoside protects RGCs, is also still unclear. Therefore, in this study, we aimed to use proteomics to understand the main molecular mechanisms of acteoside in spontaneous glaucoma to support its use as an RGC-protecting agent for the prevention of glaucoma-related blindness.

MATERIALS AND METHODS

Ethical Approval All experimental operations were in compliance with the National Institute of Health Laboratory Animal Care and Use Guidelines. The use of laboratory animals followed the relevant regulations of Tianjin Medical University and Association for Research in Vision and Ophthalmology (ARVO) on the use of animals in ophthalmology and vision science research. All experiments were approved by the Animal Care and Use Committee of Tianjin Medical University Eye Hospital (No.TJYY20181217002).

Animals Twenty female DBA/2J mice (8wk of age) and thirty female C57BL/6 mice (8wk of age) were purchased from Shanghai Slack Company. All mice were raised in a specific pathogen-free (SPF) breeding environmental animal room of the Tianjin Medical University Eye Hospital. The room temperature was 22℃–26℃ under 12-hour light-dark cycles.

IOP Measurement First, 0.4% oxybuprocaine hydrochloride (Santen, Hyogo, Japan) eye drops were applied to the ocular surface. IOP was measured with a TonoVet® (Icare Finland Oy, Helsinki, Finland) animal tonometer. The IOP of the mice was monitored every week. During the measurement process, the probe was in vertical contact with the center of the cornea. Five consecutive IOP values were measured and repeated three times. To eliminate the influence of day and night fluctuations on IOP, the measurements were taken between 2 and 4 *p.m.* every Monday afternoon. All the IOP measurements were performed by a single examiner to ensure the accuracy of the results.

Slit-Lamp Biomicroscopic Examination The mouse anterior segment was observed with a slit lamp biological microscope, and pictures were taken with an attached Nikon D90 camera (Nikon, Tokyo, Japan). The same camera and lighting parameters were used to take photos. The objective lens magnification was 10×, and 40× pictures were collected and stored in TIFF format.

Gavage Animals were divided into three groups (n=6). The normal control group was C57 mice, the saline group was the DBA-H mice gavaged with saline, and the acteoside group was the DBA-H mice gavaged with acteoside. The gavage started at 36wk and lasted for one month. Physiological saline (Otsuka Pharmaceutical Co., Ltd., Tianjin, China) was used to configure acteoside (Pusi Biotechnology Co., Ltd., Chengdu, China) to a final concentration of 18 mg/mL. For better dissolution, 3% dimethyl sulfoxide (DMSO) was added. Similarly, 3% DMSO was added to the saline group for consistency. The prepared physiological saline and acteoside solutions were drawn and gavaged according to the standard of 8.3 μL/g every day[22].

Electroretinogram Evaluation To evaluate the impact of acteoside on retinal function, electroretinogram (ERG) and visual evoked potential (VEP) were used. ERG included scotopic (dark adaptation, DA) and photopic (light adaptation, LA) conditions. The ERG a-wave and b-wave respectively reflected the function of photoreceptor cells and Müller cells[27]. After 4wk of gavage, the mice were subjected to scotopic ERG (ChongQing IRC Medical Equipment, Chongqing, China) analyses[28]. In brief, the animals were placed in darkness for 16h for DA and all procedures were performed under dim red light. The mice were anesthetized, then were fixed on a platform and their pupils were dilated with 1% tropicamide (Alcon, TX, USA). Platinum needle electrodes were placed at the center of the corneas of both eyes according to the instructions. The reference electrode was inserted into the skin between the ears, while the ground electrode was inserted into the skin near the tip of the tail. RetiMINER-Visual Electrophysiology (Chongqing IRC Medical Equipment,

Chongqing, China) was used to test and record the full-field dark adaptability ERG excited by white flashes with luminance values of 0.01, 3.0, and 30.0 cd•s/m^2. A-wave amplitudes were measured from the baseline to the valley, and b-wave amplitudes were measured from a-wave valley or the baseline to the b-wave peak.

Visual Evoked Potential The mice were dark-adapted overnight and were anesthetized. According to the instructions of the RetiMINER-visual Electrophysiological recorder, the mice were given 30.0 cd•s/m^2 white flash stimulation[29]. The full-field DA F-VEP parameters were recorded, including P1 wave amplitude and P1 wave latency. The incubation period of the P1 wave was the time from the starting point to the P1 wave peak, while the P1 wave amplitude was the distance from the starting point to the P1 wave peak.

Sample Preparation and Tandem Mass Tags Protein profiling was performed in the eyes from three groups of mice: C57 group, DBA mice with low IOP (DBA-L) group, and DBA mice with high IOP (DBA-H) group. The mice were deeply anesthetized and were enucleated. Eyeballs were sent to Tianjin Deen Biotechnology Co., Ltd. for protein profile sequencing. According to the company's regulations, this was performed using reagents from the TMT duplex isobaric labeling reagent set (Thermo Fisher Scientific, Waltham, USA)[30]. Briefly, the tissue samples were ground with liquid nitrogen, lysed with lysis solution, and tested for quality control. The total protein samples were digested into peptides. Digested proteins (~1 μg/μL) were incubated with TMT reagent (Thermo Fisher Scientific, Waltham, USA) for 1h at room temperature, which marked all the obtained peptides.

Liquid Chromatography and Mass Spectrometer Analysis Separation was performed using the nano-upgraded flow high performance liquid chromatography (HPLC) liquid phase system Easy nLC[31]. The A solution was a 0.1% formic acid aqueous solution and the B solution was a 0.1% formic acid acetonitrile aqueous solution (acetonitrile is 84%). The column was equilibrated with 95% A liquid. Samples were loaded on the chromatographic column, then separated by the analytical column at a flow rate of 300 nL/min. After chromatographic separation, the peptides were analyzed on a Q-Exactive mass spectrometer (Thermo Fisher Scientific, Waltham, USA).

Analysis of Differentially Expressed Proteins Proteome Discoverer 2.1 software (Thermo Fisher Scientific, Waltham, USA) was used for quantitative analysis[32]. The difference between groups was had a standard deviation (SD) value of 0.25 as the standard. Double SD value (0.50) was used to determine different protein expression patterns. Among them, $-1.20<Log_2<1.20$ was regarded as a differentially expressed protein. Gene ontology (GO) annotations were performed on the target differentially expressed proteins, and the EBI database was searched for conservative motifs (motifs) matching the target protein to further supplement the annotation information. GO annotation classifies proteins from three aspects: biological process (BP), molecular function (MF), and cell component (CC)[33]. In this study, target proteins were annotated using the Kyoto Encyclopedia of Genes and Genomes (KEGG) database.

Hematoxylin and Eosin Staining At 40wk, the mice were sacrificed, and the eyeballs from the normal control, saline, and acteoside groups (6 mice/group) were completely removed. The eyes were fixed in 10% formalin overnight, embedded in paraffin, and sectioned serially (3 μm). Fifteen slices of comparable positions for each eyeball were selected and stained with hematoxylin and eosin (H&E). Sections were observed under a BX51 microscope (Olympus Optical Co. Ltd., Tokyo, Japan) and pictures were taken using the cellSens Standard electronic system (Olympus Optical Co. Ltd.). The photoreceptor outer segment (OS), outer nuclear layer (ONL), outer plexiform layer (OPL), inner nuclear layer (INL), inner plexiform layer (IPL), ganglion cell layer (GCL), and total retina thickness were measured in each picture. Image J software (National Institutes of Health, Bethesda, MD, USA) was used to count the number of cells in each group of GCL per unit length.

Immunohistochemistry Immunohistochemistry (IHC) [34] was also conducted to verify the differentially expressed proteins. Briefly, paraffin sections were deparaffinized, then incubated with a rabbit anti-mouse Serta domain-containing protein 4 (Sertad4) antibody (1:100, biorbyt, Wuhan, China) at 4°C overnight. Sections were washed and incubated with the secondary antibody (1:100, Alexa Fluor 488 goat anti-rabbit, Abcam, Cambridge, UK) for 2h at room temperature. Stained sections were observed under a BX51 microscope (Olympus Optical Co. Ltd., Tokyo, Japan) and pictures were taken using the cellSens Standard electronic system. Staining intensity was examined using Image J software (National Institute of Health, Bethesda, USA). Fifteen pictures covering each section of the retina GCL, INL, and ONL were analyzed.

Cell Culture and Treatment Retinal ganglion cell 5 (RGC5; BNCC, Beijing, China) were cultured in Ham's F-12k (Gibco, Grand Island, USA) containing 10% fetal bovine serum (Thermo Fisher Scientific, Waltham, USA), 100 U/mL penicillin, and 100 μg/mL streptomycin in a humidified atmosphere of 95% O_2 and 5% CO_2 at 37°C. Cells were passaged using TrypLE™ Express (Gibco, Grand Island, USA) every two days. Cells were divided into three groups: control, glutamate and L-buthionine-sulfoximine (BSO)-treated, and glutamate plus BSO and acteoside-treated cells. The reagents were as follows: 10 mmol/L glutamate (Gibco, Grand Island, USA),

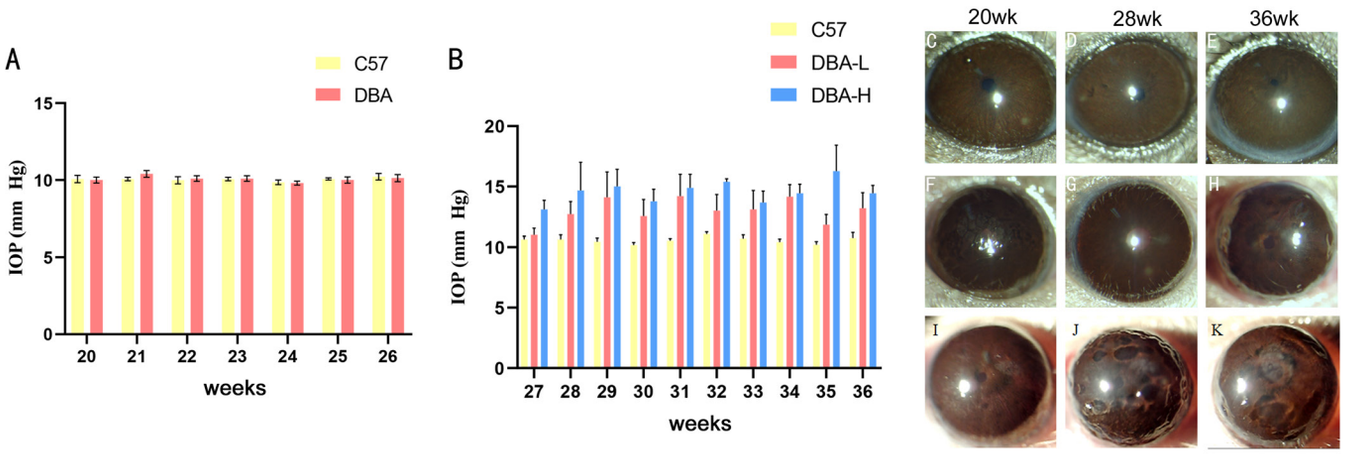

Figure 1 The three groups were the C57 mice group, the DBA mice with low IOP (DBA-L) group and the DBA mice with high IOP (DBA-H) group respectively A: The IOP of three groups of mice from 20 to 26wk; B: The IOP of three groups of mice from 27 to 36wk; C–K: Anterior segment status of three groups of mice at 20, 28, and 36wk. The three groups were C57 mice group (C–E), DBA-L group (F–H), and DBA-H group (I–K) respectively. *n*=10. The mean IOP of the DBA-L group eyes and the DBA-H eyes was 12.3±0.8 and 16.5±0.5 mm Hg, respectively. IOP: Intraocular pressure; SEM: Standard error of the mean.

0.5 μmol/L BSO (Meilunbio, Liaoning, China), and 50 μmol/L acteoside[35].

Cell Viability Measurement Cell counting kit-8 (CCK-8) assay (Dojindo Laboratories, Kumamoto, Japan) was used to assess RGC5 cell proliferation according to the manufacturer's protocol[36]. After grouping, RGC5 cells were seeded into 96-well plates at a density of 8000 cells/well per group. Then, 10 μL of CCK-8 solution was added to each well. Plates were incubated at 37°C for 3h. Finally, the optical density (OD) value of each well was examined at 450 nm using a spectrophotometer.

RNA Isolation and Quantitative Real-time PCR Assay Total RNA was isolated and extracted from cells using the RNAprep pure Micro Kit (TIANGEN, Beijing, China) according to the manufacturer's instructions[37]. About 1 μg total RNA from each sample was reverse transcribed into cDNA with the Revertaid 1St cDNA Synth Kit (Ea Thermo Fisher Scientific, Waltham, USA) in a total volume of 10 μL. Then, quantitative reverse transcription-polymerase chain reaction (qRT-PCR) was performed using EvaGreen 2X qPCR MasterMix-ROX. Reactions were 10 μL in volume and contained 5 μL SYBR Green, 0.6 μL primer pair, 1.4 μL H_2O, and 3 μL cDNA. GAPDH was used as the control gene for normalization. The primer sequences used were as follows: Data analysis was performed using the $2^{-\Delta\Delta Ct}$ method for relative gene expression.

Western Blot Analysis Cells used for Western blot[38] analysis were cultured in 6-well plates. Total protein samples were extracted using RIPA lysis buffer (CWBIO, Beijing, China) and protease inhibitor cocktail (CWBIO, Beijing, China) following the manufacturer's protocol. Proteins were separated on an 8% sodium dodecyl sulfate polyacrylamide gel and transferred to a PVDF membrane. The blot was blocked with 5% non-fat dry milk, then incubated with the anti-Sertad4 primary antibody (1:1000, biorbyt, Wuhan, China) overnight at 4°C. The blot was washed three times, then incubated with a horseradish peroxidase (HRP)-conjugated secondary antibody (1:10 000, Abcam, Cambrige, USA). The optical densities of the Sertad4 and GAPDH bands were quantified using Image J software.

Statistical Analysis All data were expressed as the mean±standard error of the mean (SEM). The differences between groups were analyzed by *t*-tests. One-way analysis of variance (ANOVA) was used when comparing more than two groups at one time-point, while two-way ANOVA was used when comparing more than two groups in a time-course. Statistical analyses were performed using GraphPad Prism 8.0 software (GraphPad Inc., San Diego, CA, USA). Differences were defined statistically significant when $P<0.05$.

RESULTS

Monitoring DBA/2J of Glaucoma As the mice grew, we observed changes in IOP and the anterior segment. IOP≥15 mm Hg was considered elevated[39]. The IOP values of the three groups of mice were all about 10 mm Hg before 26wk (Figure 1A). After 26wk, some mice had slight IOP elevation between 10 and 15 mm Hg. These mice were grouped as DBA-L, with an average IOP of 12.3±0.8 mm Hg. The other group had substantial IOP elevation (IOP higher than 15 mm Hg) and were grouped as DBA-H, with an average IOP of 16.5±0.5 mm Hg (Figure 1B). The anterior segment status was related to IOP. Compared with the DBA-L group, the anterior segment status of the DBA-H group was worse and the iris fold was more obvious (Figure 1C–1K).

Liquid Chromatography and Mass Spectrometer Analysis We then used protein profiling to further explore

the mechanism. Compared with the normal control group, the DBA-H group had 2790 significantly differentially expressed proteins, including 1445 upregulated and 1345 downregulated proteins (Figure 2G). GO analysis results, shown in Figure 2, revealed the BP, CC, and MF. The differentially expressed proteins were enriched mainly in the extracellular vesicle, membrane-bounded organelle, organelle, exosome, cytoplasm, and cytoplasmic part. The main cellular functions of all differentially expressed proteins were protein binding, macromolecular complex binding, cell adhesion molecule binding, identical protein binding, enzyme binding, cadherin binding, and RNA binding. All differentially expressed proteins were enriched mainly in the BP of cellular component organization or biogenesis, cellular component organization, organonitrogen compound metabolic process, single-organism metabolic process, and cellular component biogenesis. Using KEGG enrichment analysis, we identified the relevant signaling pathways by examining all significantly differentially expressed proteins (Figure 2D). When comparing the DBA-H and normal control groups, significantly differentially expressed proteins are listed in Figure 2E–2F. The top 20 upregulated and downregulated proteins are listed in Table 1. Sertad4 was a significantly differentially expressed protein. Elevated IOP in DBA/2J is a key factor for determining the success of the model. To prevent the influence of species differences on the protein expression profiles, we compared the DBA-H and DBA-L groups simultaneously and analyzed the differentially expressed proteins (Figure 3). The results suggested that Sertad4 was the most significantly differentially expressed protein in both groups (Table 2).

Acteoside Reduces IOP and Improves Anterior Segment Status From the previous data, we selected the DBA-H mice for the subsequent experiments. Acteoside is a water-soluble phenethyl glycoside compound (Figure 4A)[40]. After gavage administration to the mice, acteoside is rapidly absorbed and widely distributed, with good bioavailability. The gavage volume was calculated according to mice body weight. The three groups of mice were weighed daily (Figure 4B). Saline and acteoside solution (8.3 μL/g) was used for gavage once a day, with a dosage of 200 μL (Figure 4C). IOP was continuously monitored weekly. The average IOP value of the normal control group IOP was about 10 mm Hg, while those of the saline and acteoside groups were 17±0.4 and 14.9±0.5 mm Hg, respectively. These results suggested that the mice IOP could be effectively decreased after acteoside treatment (P<0.001; Figure 4D). Additionally, acteoside treatment could significantly improve the anterior segment status (Figure 4E).

Acteoside Presents Neuroprotective Effects After 4wk of gavage, the mice were euthanized and their eyes were enucleated. We examined the retina using histopathological staining (Figure 5A–5C). The overall retina thickness and that of each layer were measured. Compared with the normal control group, the retinas of the saline group mice were thinner (P<0.001). After acteoside treatment, however, this was significantly improved (P<0.001). The GCL cell number was also calculated. Compared with the normal control group, the saline group GCL cell number was significantly decreased (P<0.0001), but was significantly increased following acteoside treatment (P<0.01). Overall, acteoside treatment demonstrated neuroprotective effects in our study (Figure 5D, 5E).

Table 1 Significantly different gene statistics (DBA-H group *vs* C57 mice)

UniProt ID	Gene name	Log2 FC	*Q*-value	Up/down
A0A0A6YXT5	*Sertad4*	11.10	0.0088687	Up
G5E8J6	*Hrc*	10.10	0.0076805	Up
O88662	*Emp2*	10.07	0.0020896	Up
Q9JI33	*Ntn4*	9.89	0	Up
F6TYB7	*Mbp*	9.85	0.00024254	Up
Q91ZQ1-2	*Pde6c*	9.74	0	Up
D3Z6B9	*Aldh1l2*	9.47	0.00024426	Up
D3Z6G3	*Mapre3*	8.89	0.00024826	Up
Q80SY9	*Nod2*	8.84	0.0076353	Up
Q8VBT9	*Aspscr1*	8.72	0	Up
P97427	*Crmp1*	8.71	0.00024685	Up
Q50H33-2	*Kctd8*	8.54	0.00048008	Up
Q8K3X6	*Anks4b*	8.40	1	Up
A6XDB1	*Pde4d*	8.29	0	Up
Q8VCX5	*Micu1*	8.22	0	Up
Q8K3W3	*Casc3*	8.21	0.0045045	Up
Q8BUR4	*Dock1*	8.16	0.00025478	Up
Q99J39-2	*Mlycd*	8.16	0.00024919	Up
P62715	*Ppp2cb*	8.15	0	Up
Q99L27	*Gmpr2*	8.11	0.0018657	Up
P07724	*Alb*	10.00	0	Down
A2ASS6	*Ttn*	9.25	0	Down
Q5SX39	*Myh4*	9.22	0	Down
Q921I1	*Tf*	8.51	0	Down
P24622	*Cryaa*	8.33	0	Down
P24622-2	*Cryaa*	8.10	0	Down
P07759	*Serpina3k*	7.96	0	Down
E9Q1W3	*Neb*	7.89	0	Down
P01027	*C3*	7.70	0	Down
Q61838	*A2m*	7.49	0	Down
P28665	*Mug1*	7.07	0	Down
E9Q616	*Ahnak*	7.07	0	Down
P07310	*Ckm*	7.04	0	Down
B7FAU9	*Flna*	6.97	0	Down
Q8R429	*Atp2a1*	6.86	0	Down
P35441	*Thbs1*	6.85	0	Down
Q91X72	*Hpx*	6.85	0	Down
Q5SX40	*Myh1*	6.84	0	Down
Q8VDD5	*Myh9*	6.79	0	Down
P16858	*Gapdh*	6.78	0	Down

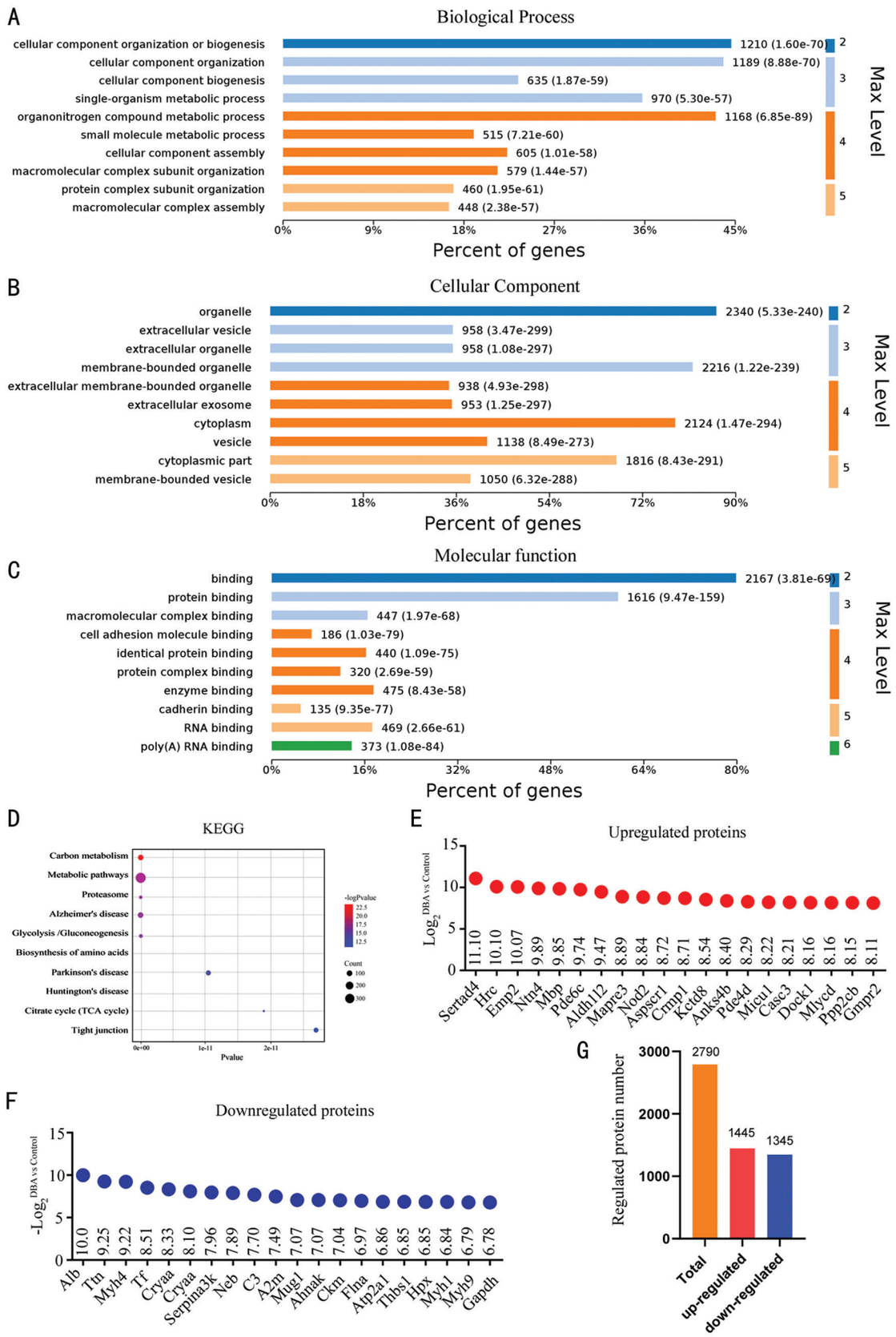

Figure 2 Proteomics analysis between DBA-H and normal control groups A–C: Gene ontology analysis of significantly expressed proteins in DBA-H group compared with normal control group. GO analysis mainly includes three aspects: biological process, cellular component, and molecular function. D: Analysis of the KEGG pathway. E: Top 20 up-regulated expression proteins. F: Top 20 down-regulated expression proteins. G: The number of significantly regulated protein. DBA-H: DBA mice with high intraocular pressure; KEGG: Kyoto Encyclopedia of Genes and Genomes.

Retinal Functional Assessment by Visual Function DA 0.01, DA 3.0, and DA 30.0 ERG were tested. The representative wave forms and corresponding amplitudes of VEP and ERG at 40wk are shown in Figure 6. No significant changes in DA

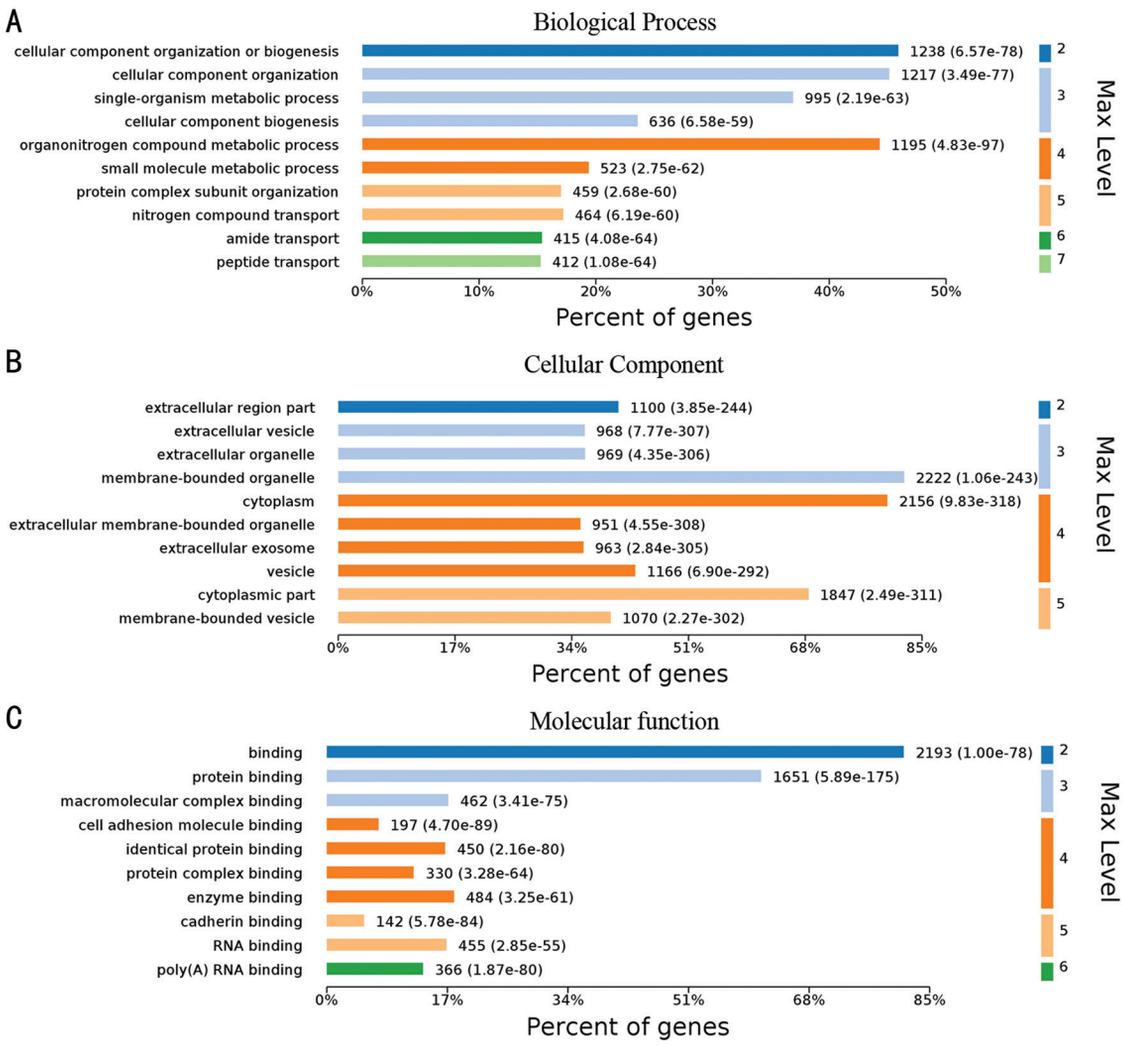

Figure 3 Gene ontology analysis of significantly differentially expressed proteins between DBA-H group and DBA-L group, including biological process (A), cellular component, cellular component (B), and molecular function (C). DBA-H: DBA mice with high IOP; IOP: Intraocular pressure; DBA-L: DBA mice with low IOP.

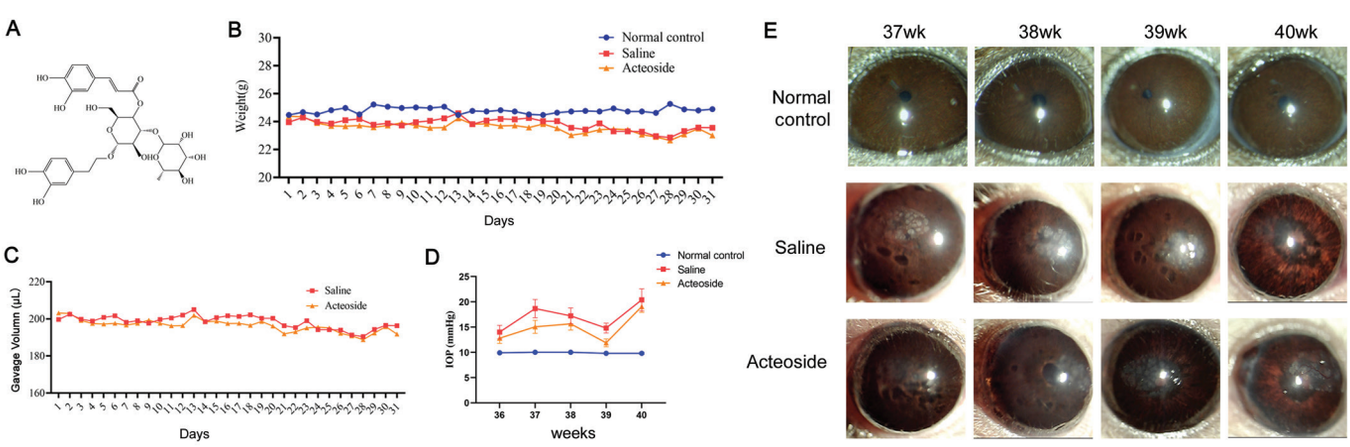

Figure 4 IOP and anterior segment of mice over 4wk observation time A: Molecular structures of acteoside; B: Weight of mice at different times; C: The amount of gavage at different times; D: The IOP in three groups of mice over 4wk observation time. The mean IOP of the DBA-L group eyes and the DBA-H eyes was 17.0±0.4 and 14.9±0.5 mm Hg, respectively (P<0.001). E: Effects of gavage on the anterior segment of mice over 4wk observation time. Error bars indicate SEM. IOP: Intraocular pressure; SEM: Standard error of the mean; DBA-H: DBA mice with high IOP; DBA-L: DBA mice with low IOP.

0.01, DA 3, or DA 30.0 were observed in the three groups (P>0.05; Figure 6F), indicating that there were normal retina and photoreceptor functions under scotopic environment. The b-waves of the three groups were not statistically different and

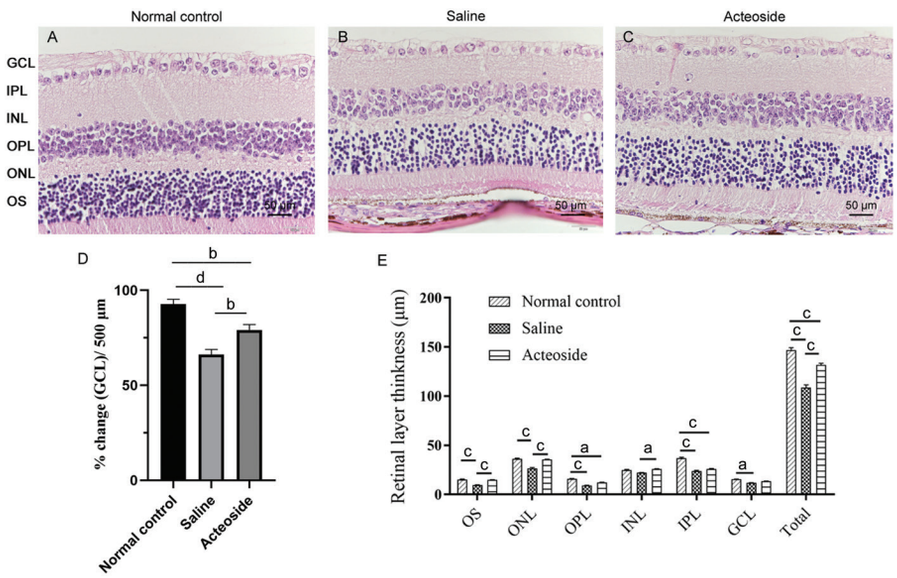

Figure 5 The histological analysis of mice eyes at 40wk The three groups were respectively normal control group (A), saline group (B) and acteoside group (C). D: Histological analysis GCL counts in retinas. E: The thickness of each layer of the retina in the three groups of mice. [a]*P*<0.05; [b]*P*<0.01, [c]*P*<0.001, [d]*P*<0.0001. Error bars indicate SEM. GCL: Ganglion cell layer; IPL: Inner plexiform layer; INL: Inner nuclear layer; OPL: Outer plexiform layer; ONL: Outer nuclear layer; OS: Outer segment; SEM: Standard error of the mean.

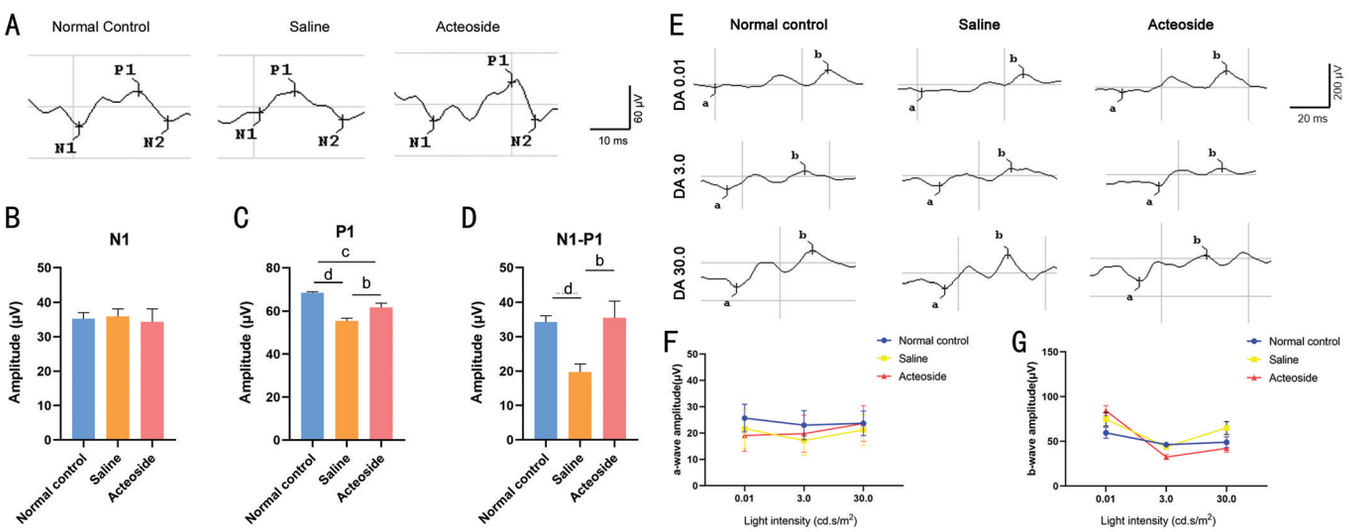

Figure 6 The retinal function examinations of mice eyes at 40wk A: VEP tests waves of normal control group, saline group and acteoside group. B-D: The amplitude of N1 (B), P1 (C), N1-P1 (D) in three groups. E: Waveforms of dark-adapted 0.01 ERG (DA 0.01 ERG) tests, dark-adapted 3.0 ERG (DA 3.0 ERG) tests and dark-adapted 30.0 ERG (DA 30.0 ERG) tests for normal control, saline and acteoside group. F: A-wave amplitudes recorded in DA 0.01, DA 3, DA 30.0 ERG tests. G: B-wave amplitudes recorded in DA 0.01, DA 3, DA 30.0 ERG tests. The aforementioned 0.01, 3.0 and 30.0 respectively represented 0.01, 2.562, and 25.62 cd•s/m^2 stimulus in ERG tests. [b]*P*<0.01, [c]*P*<0.001, [d]*P*<0.0001. Error bars indicate SEM. VEP: Visual evoked potential; DA: Dark adaptation; ERG: Electroretinogram; LA: Light adaptation; SEM: Standard error of the mean.

all amplitudes were within a normal range (*P*>0.05; Figure 6G). All mice received the VEP test (Figure 6A). The N1 waves had no significant changes among the three groups (*P*>0.05; Figure 6B). Compared with the normal control group, the P1 wave of the saline group was decreased, while acteoside treatment could improve this condition (Figure 6C). The variation trend of N1-P1 wave was similar to that of P1 (Figure 6D).

Protein Expression Validation with Immunohistochemistry

IHC staining was conducted to validate the expression patterns of the proteins selected by mass spectrometry. IHC was performed after 4wk of gavage. Retina tissue sections were incubated with an Sertad4 antibody. As shown in Figure 7, Sertad4 expression was observed in the normal control group. The whole retina average OD was increased in the saline group (*P*<0.0001; Figure 7D). This indicated that Sertad4 protein expression levels were increased in the saline group, which was consistent with our previous results. Compared with the saline group, the mean OD was significantly decreased after acteoside treatment, suggesting that acteoside could effectively

Table 2 Significantly different gene statistics (DBA-H group *vs* DBA-L group)

UniProt ID	Gene name	Log_2 FC	*Q*-value	Up/down
A0A0A6YXT5	*Sertad4*	13.76	0.0088687	Up
A0A140LHT4	*GM9195*	12.57	0.00024637	Up
G5E8J6	*Hrc*	11.35	0.0076805	Up
Q80SY9	*Nod2*	11.08	0.0076353	Up
Q91ZQ1-2	*Pde6c*	11.08	0	Up
Q9JI33	*Ntn4*	11.07	0	Up
F6TYB7	*Mbp*	11.05	0.00024254	Up
O88662	*Emp2*	10.83	0.0020896	Up
E9QQ68	*Tbc1d12*	10.49	0.0062029	Up
P97427	*Crmp1*	10.26	0.00024685	Up
Q8VCX5	*Micu1*	10.10	0	Up
D3Z6B9	*Aldh1l2*	10.03	0.00024426	Up
D3Z6G3	*Mapre3*	9.81	0.00024826	Up
B1AYG6	*Itgb6*	9.75	0.0062112	Up
A6XDB1	*Pde4d*	9.74	0	Up
P02802	*Mt1*	9.70	0	Up
Q8K3X6	*Anks4b*	9.51	1	Up
Q8K3W3	*Casc3*	9.29	0.0045045	Up
Q642K5	*Fau*	9.21	0.0034215	Up
Q99L27	*Gmpr2*	9.20	0.0018657	Up
P07724	*Alb*	10.96	0	Down
P07759	*Serpina3k*	9.73	0	Down
Q5SX39	*Myh4*	9.53	0	Down
Q921I1	*Tf*	9.37	0	Down
A2ASS6	*Ttn*	9.33	0	Down
P24622	*Cryaa*	9.18	0	Down
P04104	*Krt1*	8.73	0	Down
P01027	*C3*	8.55	0	Down
Q61838	*A2m*	8.47	0	Down
P28665	*Mug1*	8.28	0	Down
P24622-2	*Cryaa*	8.23	0	Down
E9Q1W3	*Neb*	8.12	0	Down
P02089	*Hbb-b2*	8.02	0	Down
Q61646	*Hp*	7.94	0	Down
P35441	*Thbs1*	7.85	0	Down
Q91X72	*Hpx*	7.80	0	Down
A0A0R4J0X5	*Serpina1a*	7.78	0	Down
P02088	*Hbb-b1*	7.63	0	Down
Q61781	*Krt14*	7.37	0	Down
B7FAU9	*Flna*	7.31	0	Down

inhibit Sertad4 expression (P<0.01). Additionally, the GCL, INL, and ONL showed similar trends (Figure 7E). Combined with our previous data, these results implied that acteoside possibly exerts its function by downregulating Sertad4 expression. Collectively, these findings showed that Sertad4 may be a potential target of acteoside.

Acteoside Relieves Cell Injury in Glutamate-Induced RGC5 Cells *via* Sertad4 In this study, we used 10 mmol/L glutamate, 0.5 μmol/L BSO, and 50 μmol/L acteoside. As shown in Figure 8A, 8B, cell metabolism and proliferation were affected by glutamate stimulation. Furthermore, acteoside could support effective resistance to oxidative stress. We used qRT-PCR to examine Sertad4 mRNA expression levels in the three groups (Figure 8C). After glutamate treatment, Sertad4 mRNA levels were significantly upregulated (P<0.0001), which was consistent with our animal experiment results. However, Sertad4 mRNA levels were significantly downregulated following acteoside treatment (P<0.0001), indicating that acteoside might play a protective role. Similarly, we verified Sertad4 protein expression levels (Figure 8D). Compared with the saline group, Sertad4 protein expression levels were significantly decreased in the acteoside group (P<0.01). The relative density statistics of protein reflected this intuitively (Figure 8E).

DISCUSSION

Glaucoma is the second leading cause of blindness worldwide. It is characterized by optic atrophy and visual field defects. Elevated IOP and RGC damage are generally considered to be the main causes of glaucoma[41]. In our study, the DBA/2J mouse model with elevated IOP showed some typical features of glaucoma[42]. As the DBA/2J mice grew with age, they showed iris pigment diffusion, which led to anterior chamber angle closure and elevated IOP. This phenomenon was of great interest to us. We therefore aimed to identify the key functional proteins associated with this disease model using protein mass spectrometry analysis.

In our results, Sertad4 was the most differentially expressed upregulated protein. We thus speculated that it is potentially important for glaucoma development. Sertad4 belongs to the Sertad family of proteins, which includes Sertad1, Sertad2, Sertad3, and Sertad4. Sertad4 is a newly discovered protein and its function is not fully clear at present. The main functions of this protein are related to vascular adventitial fibroblasts[43], cardiac development, and bone mineral density. The Serta domain has been demonstrated to have different regulatory effects on the development of drosophila neural lineage[44]. This domain is highly conserved among species and may play a similar role in mammals. The development and pathological death of neurons require activation of specific cell cycle pathways. Proteins containing a Serta domain have also been shown to participate in cell cycle progression[45]. Sertad2 is expressed in the retina. Genetic analysis of retinitis pigmentosa (RP) in an Indian family suggested that Sertad2 might be the key gene in this disease[46]. Sertad3 is overexpressed in retinoblastoma by magnetic resonance analysis[47]. Studies have shown that Sertad1 may have neuroprotective functions.

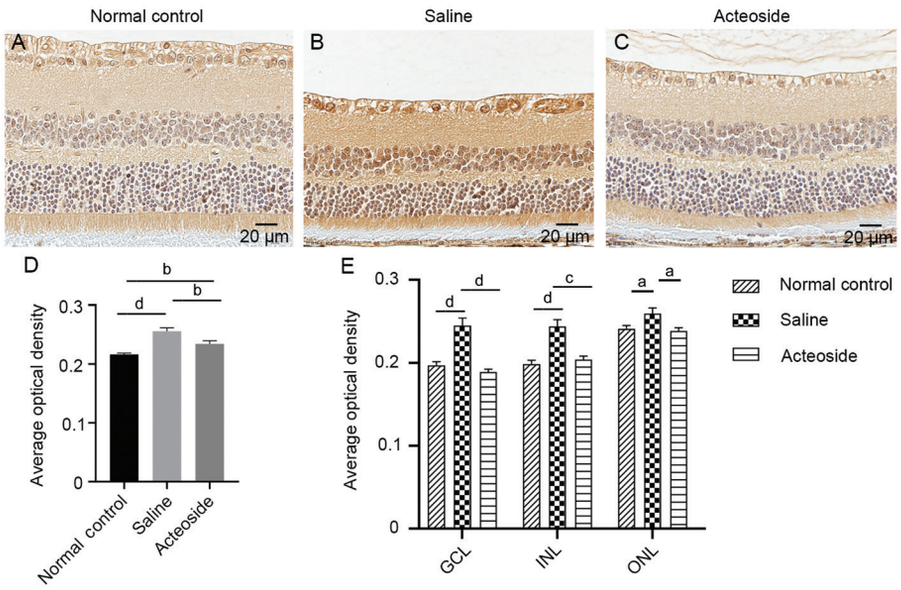

Figure 7 The immunohistochemistry of mice eyes at 40wk Expression of Sertad4 in normal control group (A), saline group (B) and acteoside group (C). D: Statistics of the average optical density values of the three groups. E: Statistics of the average optical density values of the three groups of GCL, INL, and ONL. [a]*P*<0.05; [b]*P*<0.01, [c]*P*<0.001, [d]*P*<0.0001. Error bars indicate SEM. GCL: Ganglion cell layer; INL: Inner nuclear layer; ONL: Outer nuclear layer; SEM: Standard error of the mean.

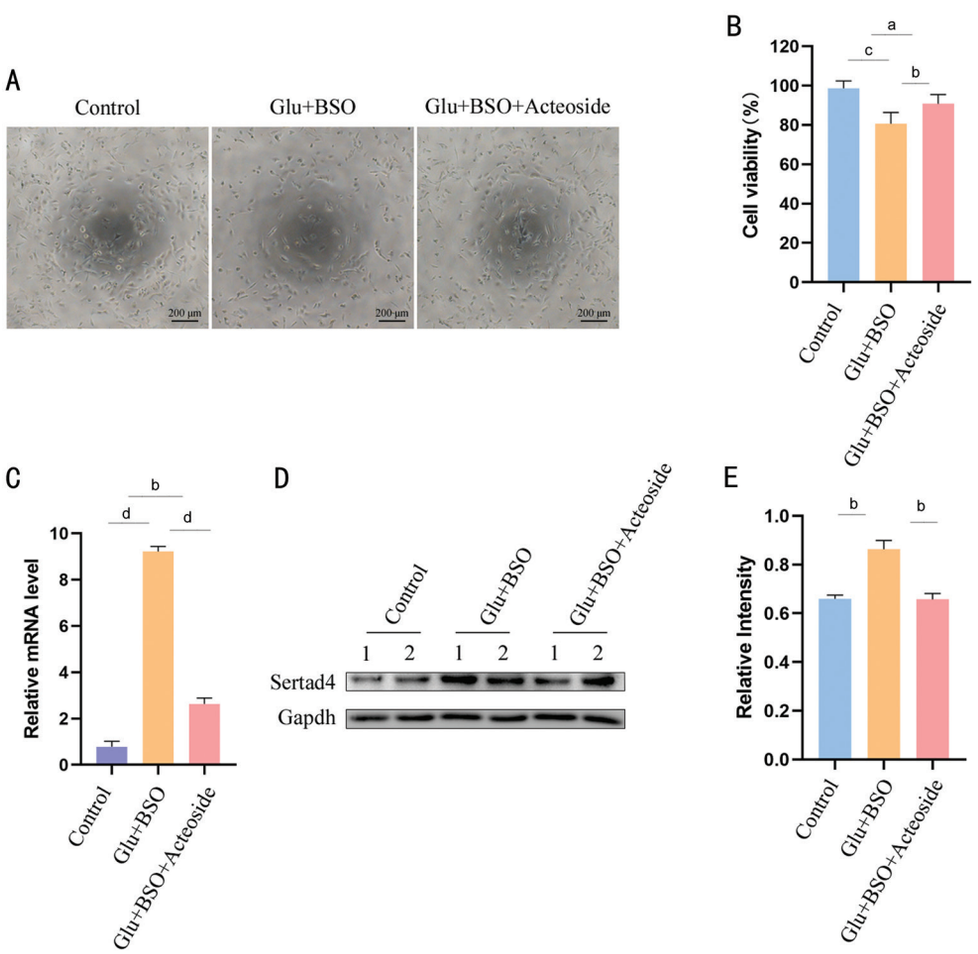

Figure 8 Acteoside relieves cell injury in RGC5 *via* Sertad4 A: Three groups of cells were observed under a microscope to assess cell number and growth status; B: Cell viability of the three groups. C: The relative expression levels of Sertad4 genes in three group cells. D: Western blot representatives of Sertad4 and GAPDH in three groups. Two replicate wells were set for each group. E: Ratio of Sertad4 over GAPDH in three groups. [a]*P*<0.05; [b]*P*<0.01, [c]*P*<0.001, [d]*P*<0.0001. Error bars indicate SEM. GAPDH: Glyceraldehyde-3-phosphate dehydrogenase; SEM: Standard error of the mean; RGC5: Retinal ganglion cell 5.

Upregulation of Sertad1 was observed in Alzheimer's disease, leading to neuronal death. Additionally, Sertad1 knockdown can significantly improve neurological deficit and neuronal apoptosis[48]. This protein is also critical for neuronal death induced by nerve growth factor withdrawal and beta-amyloid in the cerebral cortex[49]. Taken together, we speculate that Sertad4 likely has neuroprotective functions.

Acteoside has a variety of biological activities *in vitro* and *in vivo*, such as antioxidant stress injury neuroprotection, anti-inflammatory properties, and anti-apoptosis effects. Acteoside showed neuroprotective functions in different animal models. Ji *et al*[50] found that acteoside significantly alleviated the mice cognitive deficit in the Y-maze test and the neuronal damage in the hippocampal CA1 area. Yuan *et al*[51] found that acteoside and caspase-3 played a neuroprotective role in PD rat model. Xi *et al*[52] have found that acteoside can attenuate RGC loss and oxidative stress by activating PI3K/AKT signaling in the ocular hypertension (HP) rat model.

In vitro cell data suggested that acteoside had a significant neuroprotective effect on glutamate-induced neurotoxicity in primary cultured rat cortical cells[27]. Acteoside could also attenuate RGC autophagy and apoptosis through the miR-155/mTOR axis[53] and the OPTN and PI3K/AKT/mTOR pathway[54]. However, there is no evidence that acteoside has neuroprotective effects in spontaneous glaucoma mice.

In our study, IOP decreased after acteoside treatment. H&E staining results showed that acteoside treatment significantly improved the total retina thickness, especially the RGC layer cell number. These results preliminarily suggested that acteoside has neuroprotective effects in the DBA/2J mouse model. We also observed a clear reduction of iris pigment diffusion in the acteoside-treated group. We speculate that acteoside can improve the diffusion of pigment, alleviate the obstruction of the anterior chamber angle, and enhance the aqueous humor circulation. This collectively leads to IOP reduction. Acteoside could also improve the N1-P1 and P1 values. Our results showed that acteoside could protect the retina and improve visual function. Cell viability was significantly increased following acteoside treatment, indicating that acteoside could protect RGC5 by inhibiting oxidative stress. Sertad4 protein expression levels were significantly increased, as seen with IHC assays, which was consistent with our previous protein mass spectrometry results. Therefore, we speculated that acteoside may play a key role in neuroprotection through Sertad4. The findings presented in this study can pave the way to systematic translational approaches to uncover the role of Sertad4 in glaucoma and evaluate its potential as a target of acteoside. Our findings suggest that acteoside could possibly be used for glaucoma treatment, though further experiments are needed to clarify the specific molecular mechanism. These results provide new insights for medical interventions in glaucoma.

In conclusion, we determined the effects of acteoside treatment in a glaucoma mouse model. Sertad4 is differentially expressed in DBA/2J mice. Acteoside protects RGCs from damage, possibly through the downregulation of Sertad4, and has potential use in glaucoma treatment.

ACKNOWLEDGEMENTS

We acknowledge and appreciate our colleagues for their valuable efforts and comments on this paper. We thank J. Iacona, Ph.D., from Liwen Bianji (Edanz) (www.liwenbianji.cn), for editing the English text of a draft of this manuscript.

Foundation: Supported by Tianjin Key Medical Discipline (Specialty) Construction Project (No.TJYXZDXK-037A).

Conflicts of Interest: Hao HJ, None; **Li YH,** None; **Yu B,** None; **Liu X,** None; **Zhang Y,** None; **Xing XL,** None.

REFERENCES

1 Rashidian P. Race in the phenotype of glaucoma: genotypic or environmental variance? *Med Hypothesis Discov Innov Optom* 2021;2(4):161-162.

2 Shen F, Chen B, Danias J, Lee KC, Lee H, Su YL, Podos SM, Mittag TW. Glutamate-induced glutamine synthetase expression in retinal Muller cells after short-term ocular hypertension in the rat. *Invest Ophthalmol Vis Sci* 2004;45(9):3107-3112.

3 Libby RT, Anderson MG, Pang IH, *et al*. Inherited glaucoma in DBA/2J mice: pertinent disease features for studying the neurodegeneration. *Vis Neurosci* 2005;22(5):637-648.

4 Buonfiglio F, Pfeiffer N, Gericke A. Immunomodulatory and antioxidant drugs in glaucoma treatment. *Pharmaceuticals* (*Basel*) 2023;16(9):1193.

5 Al-Namaeh M. Pharmaceutical treatment of primary open angle glaucoma. *Med Hypothesis Discov Innov Optom* 2021;2(1):8-17.

6 Alipieva K, Korkina L, Orhan IE, Georgiev MI. Verbascoside—a review of its occurrence, (bio)synthesis and pharmacological significance. *Biotechnol Adv* 2014;32(6):1065-1076.

7 Wu YT, Lin LC, Sung JS, Tsai TH. Determination of acteoside in Cistanche deserticola and Boschniakia rossica and its pharmacokinetics in freely-moving rats using LC-MS/MS. *J Chromatogr B Analyt Technol Biomed Life Sci* 2006;844(1):89-95.

8 Song HS, Choi MY, Ko MS, *et al*. Competitive inhibition of cytosolic Ca^{2+}-dependent phospholipase A2 by acteoside in RBL-2H3 cells. *Arch Pharm Res* 2012;35(5):905-910.

9 Lee HD, Kim JH, Pang QQ, Jung PM, Cho EJ, Lee S. Antioxidant activity and acteoside analysis of *Abeliophyllum distichum*. *Antioxidants* (*Basel*) 2020;9(11):1148.

10 Xiao YS, Ren Q, Wu LH. The pharmacokinetic property and pharmacological activity of acteoside: a review. *Biomed Pharmacother* 2022;153:113296.

11 Wang CY, Cai XY, Wang RC, Zhai SY, Zhang YF, Hu WJ, Zhang YZ, Wang D. Neuroprotective effects of verbascoside against

Alzheimer's disease via the relief of endoplasmic reticulum stress in Aβ-exposed U251 cells and APP/PS1 mice. *J Neuroinflammation* 2020;17(1):309.

12 Nawrot J, Gornowicz-Porowska J, Budzianowski J, Nowak G, Schroeder G, Kurczewska J. Medicinal herbs in the relief of neurological, cardiovascular, and respiratory symptoms after COVID-19 infection A literature review. *Cells* 2022;11(12):1897.

13 Mao Y, Yu JL, Da JJ, Yu FX, Zha Y. Acteoside alleviates UUO-induced inflammation and fibrosis by regulating the HMGN1/TLR4/TREM1 signaling pathway. *PeerJ* 2023;11:e14765.

14 Gao WY, Zhou YY, Li CY, *et al*. Studies on the metabolism and mechanism of acteoside in treating chronic glomerulonephritis. *J Ethnopharmacol* 2023;302(Pt A):115866.

15 Guo J, Liu QZ, Zhu FJ, Li M, Li J, Guo L, Sun QY, Yang QX. Acteoside attenuates acute lung injury following administration of cobra venom factor to mice. *Heliyon* 2022;8(11):e11622.

16 Mosca M, Ambrosone L, Semeraro F, Casamassima D, Vizzarri F, Costagliola C. Ocular tissues and fluids oxidative stress in hares fed on verbascoside supplement. *Int J Food Sci Nutr* 2014;65(2):235-240.

17 Ambrosone L, Guerra G, Cinelli M, *et al*. Corneal epithelial wound healing promoted by verbascoside-based liposomal eyedrops. *Biomed Res Int* 2014;2014:471642.

18 Piwowarczyk L, Mlynarczyk DT, Krajka-Kuźniak V, *et al*. Natural compounds in liposomal nanoformulations of potential clinical application in glioblastoma. *Cancers* 2022;14(24):6222.

19 Li SM, Cui YJ, Li M, Zhang WT, Sun XX, Xin ZX, Li J. Acteoside derived from cistanche improves glucocorticoid-induced osteoporosis by activating PI3K/AKT/mTOR pathway. *J Invest Surg* 2023;36(1):2154578.

20 Wang YM, Wu S, Li Q, *et al*. Salsolinol induces Parkinson's disease through activating NLRP3-dependent pyroptosis and the neuroprotective effect of acteoside. *Neurotox Res* 2022;40(6):1948-1962.

21 Al-Barghouthi BM, Mesner LD, Calabrese GM, *et al*. Systems genetics in diversity outbred mice inform BMD GWAS and identify determinants of bone strength. *Nat Commun* 2021;12(1):3408.

22 Zhao J, Liu T, Ma L, Yan M, Zhao Y, Gu ZY, Huang Y. Protective effect of acteoside on immunological liver injury induced by Bacillus Calmette-Guerin plus lipopolysaccharide. *Planta Med* 2009;75(14):1463-1469.

23 Jackson CJ, Gundersen KG, Tong L, Utheim TP. Dry eye disease and proteomics. *Ocul Surf* 2022;24:119-128.

24 Aghamollaei H, Parvin S, Shahriary A. Review of proteomics approach to eye diseases affecting the anterior segment. *J Proteomics* 2020;225:103881.

25 Zhou L, Beuerman RW. Tear analysis in ocular surface diseases. *Prog Retin Eye Res* 2012;31(6):527-550.

26 Liu XN, Wang Q, Shao ZB, Zhang SQ, Hou MY, Jiang ML, Du MX, Li J, Yuan HP. Proteomic analysis of aged and OPTN E50K retina in the development of normal tension glaucoma. *Hum Mol Genet* 2021;30(11):1030-1044.

27 Koo KA, Kim SH, Oh TH, Kim YC. Acteoside and its aglycones protect primary cultures of rat cortical cells from glutamate-induced excitotoxicity. *Life Sci* 2006;79(7):709-716.

28 Tan ZZ, Guo YJ, Shrestha M, Sun D, Gregory-Ksander M, Jakobs TC. Microglia depletion exacerbates retinal ganglion cell loss in a mouse model of glaucoma. *Exp Eye Res* 2022;225:109273.

29 Heiduschka P, Julien S, Schuettauf F, Schnichels S. Loss of retinal function in aged DBA/2J mice - New insights into retinal neurodegeneration. *Exp Eye Res* 2010;91(5):779-783.

30 Li JM, Van Vranken JG, Pontano Vaites L, *et al*. TMTpro reagents: a set of isobaric labeling mass tags enables simultaneous proteome-wide measurements across 16 samples. *Nat Methods* 2020;17(4):399-404.

31 Fan SF, Ma JM, Li CS, *et al*. Determination of tropomyosin in shrimp and crab by liquid chromatography-tandem mass spectrometry based on immunoaffinity purification. *Front Nutr* 2022;9:848294.

32 Shi YN, Wang XF, Huang AX. Proteomic analysis and food-grade enzymes of Moringa oleifer Lam. a Lam. flower. *Int J Biol Macromol* 2018;115:883-890.

33 Mai HJ, Baby D, Bauer P. Black sheep, dark horses, and colorful dogs: a review on the current state of the Gene Ontology with respect to iron homeostasis in *Arabidopsis thaliana*. *Front Plant Sci* 2023;14:1204723.

34 Xie SB, Wu YH, Hao HJ, Li JR, Guo S, Xie W, Li DW, Zhou J, Gao JM, Liu M. CYLD deficiency promotes pancreatic cancer development by causing mitotic defects. *J Cell Physiol* 2019;234(6):9723-9732.

35 Tanaka J, Nakanishi T, Shimoda H, *et al*. Purple rice extract and its constituents suppress endoplasmic reticulum stress-induced retinal damage *in vitro* and *in vivo*. *Life Sci* 2013;92(1):17-25.

36 He C, Li Y, Chen ZY, Huang CK. Crosstalk of renal cell carcinoma cells and tumor-associated macrophages aggravates tumor progression by modulating muscleblind-like protein 2/B-cell lymphoma 2/beclin 1-mediated autophagy. *Cytotherapy* 2023;25(3):298-309.

37 Wang JJ, Williams W, Wang B, *et al*. Cytotoxic effect of interleukin-8 in retinal ganglion cells and its possible mechanisms. *Int J Ophthalmol* 2018;11(8):1277-1283.

38 Hsu WH, Chung CP, Wang YY, Kuo YH, Yeh CH, Lee IJ, Lin YL. Dendrobium Nobile protects retinal cells from UV-induced oxidative stress damage via Nrf2/HO-1 and MAPK pathways. *J Ethnopharmacol* 2022;288:114886.

39 Shen JH, Wang YQ, Yao K. Protection of retinal ganglion cells in glaucoma: current status and future. *Exp Eye Res* 2021;205:108506.

40 Zhao Y, Wang SJ, Pan J, Ma K. Verbascoside: a neuroprotective phenylethanoid glycosides with anti-depressive properties. *Phytomedicine* 2023;120:155027.

41 Pu LP, Zhou RY, Li Q, Qing GP. Distribution of pigment particles in aqueous drainage structures in a DBA/2J mouse model of pigmentary glaucoma. *Invest Ophthalmol Vis Sci* 2022;63(6):2.

42 Harada C, Kimura A, Guo XL, Namekata K, Harada T. Recent advances in genetically modified animal models of glaucoma and their roles in drug repositioning. *Br J Ophthalmol* 2019;103(2):161-166.

43 Hu YC, Han T, Fan YJ, Zhang CY, Zhang Y, Ma WD, Wang CX. Urotensin II activates the ferroptosis pathway through circ0004372/miR-124/SERTAD4 to promote the activation of vascular adventitial fibroblasts. *Gen Physiol Biophys* 2022;41(5):381-392.

44 Manansala MC, Min S, Cleary MD. The Drosophila SERTAD protein Taranis determines lineage-specific neural progenitor proliferation patterns. *Dev Biol* 2013;376(2):150-162.

45 Bennetts JS, Fowles LF, Berkman JL, van Bueren KL, Richman JM, Simpson F, Wicking C. Evolutionary conservation and murine embryonic expression of the gene encoding the SERTA domain-containing protein CDCA4 (HEPP). *Gene* 2006;374:153-165.

46 Kumar A, Shetty J, Kumar B, Blanton SH. Confirmation of linkage and refinement of the RP28 locus for autosomal recessive retinitis pigmentosa on chromosome 2p14-p15 in an Indian family. *Mol Vis* 2004;10:399-402.

47 Jansen RW, de Jong MC, Kooi IE, *et al*. MR imaging features of retinoblastoma: association with gene expression profiles. *Radiology* 2018;288(2):506-515.

48 Li JX, Li B, Bu YJ, Zhang HL, Guo J, Hu JP, Zhang YF. Sertad1 induces neurological injury after ischemic stroke via the CDK4/p-Rb pathway. *Mol Cells* 2022;45(4):216-230.

49 Biswas SC, Zhang Y, Iyirhiaro G, *et al*. Sertad1 plays an essential role in developmental and pathological neuron death. *J Neurosci* 2010;30(11):3973-3982.

50 Ji SL, Cao KK, Zhao XX, Kang NX, Zhang Y, Xu QM, Yang SL, Liu YL, Wang C. Antioxidant activity of phenylethanoid glycosides on glutamate-induced neurotoxicity. *Biosci Biotechnol Biochem* 2019;83(11):2016-2026.

51 Yuan JW, Ren JP, Wang Y, He X, Zhao YW. Acteoside binds to caspase-3 and exerts neuroprotection in the rotenone rat model of Parkinson's disease. *PLoS One* 2016;11(9):e0162696.

52 Xi XT, Chen QB, Ma J, Wang XW, Xia Y, Wen XW, Cai B, Li Y. Acteoside protects retinal ganglion cells from experimental glaucoma by activating the PI3K/AKT signaling pathway via caveolin 1 upregulation. *Ann Transl Med* 2022;10(6):312.

53 Xi XT, Ma J, Chen QB, Wang XW, Xia Y, Wen XW, Yuan J, Li Y. Acteoside attenuates hydrogen peroxide-induced injury of retinal ganglion cells via the CASC2/miR-155/mTOR axis. *Ann Transl Med* 2022;10(1):5.

54 Huang KC, Gomes C, Shiga Y, *et al*. Autophagy disruption reduces mTORC1 activation leading to retinal ganglion cell neurodegeneration associated with glaucoma. *bioRxiv* 2023:2023.01.04.522687.